

HAMILTONIAN Q -LEARNING: LEVERAGING IMPORTANCE-SAMPLING FOR DATA EFFICIENT RL

Udari Madhushani[†], Biswadip Dey[‡], Naomi Ehrich Leonard[†], Amit Chakraborty[‡]

[†]Princeton University, [‡]Siemens Technology

udarim@princeton.edu, biswadip.dey@siemens.com

naomi@princeton.edu, amit.chakraborty@siemens.com

ABSTRACT

Model-free reinforcement learning (RL), in particular Q -learning is widely used to learn optimal policies for a variety of planning and control problems. However, when the underlying state-transition dynamics are stochastic and high-dimensional, Q -learning requires a large amount of data and incurs a prohibitively high computational cost. In this paper, we introduce Hamiltonian Q -Learning, a data efficient modification of the Q -learning approach, which adopts an importance-sampling based technique for computing the Q function. To exploit stochastic structure of the state-transition dynamics, we employ Hamiltonian Monte Carlo to update Q function estimates by approximating the expected future rewards using Q values associated with a subset of next states. Further, to exploit the latent low-rank structure of the dynamic system, Hamiltonian Q -Learning uses a matrix completion algorithm to reconstruct the updated Q function from Q value updates over a much smaller subset of state-action pairs. By providing an efficient way to apply Q -learning in stochastic, high-dimensional problems, the proposed approach broadens the scope of RL algorithms for real-world applications, including classical control tasks and environmental monitoring.

1 INTRODUCTION

In recent years, reinforcement learning (Sutton & Barto, 2018) have achieved remarkable success with sequential decision making tasks especially in complex, uncertain environments. RL algorithms have been widely applied to a variety of real world problems, such as resource allocation (Mao et al., 2016), chemical process optimization (Zhou et al., 2017), automatic control (Duan et al., 2016), and robotics (Kober et al., 2013). Existing RL techniques often offer satisfactory performance only when it is allowed to explore the environment long enough and generating a large amount of data in the process (Mnih et al., 2015; Kamthe & Deisenroth, 2018; Yang et al., 2020a). This can be prohibitively expensive and thereby limits the use of RL for complex decision support problems.

Q -Learning (Watkins, 1989; Watkins & Dayan, 1992) is a model-free RL framework that captures the salient features of sequential decision making, where an agent, after observing current state of the environment, chooses an action and receives a reward. The action chosen by the agent is based on a policy defined by the state-action value function, also called the Q function. Performance of such policies strongly depends on the accessibility of a sufficiently large data set covering the space spanned by the state-action pairs. In particular, for high-dimensional problems, existing model-free RL methods using random sampling techniques leads to poor performance and high computational cost. To overcome this challenge, in this paper we propose an intelligent sampling technique that exploits the inherent structures of the underlying space related to the dynamics of the system.

It has been observed that formulating planning and control tasks in a variety of dynamical systems such as video games (Atari games), classical control problems (simple pendulum, cart pole and double integrator) and adaptive sampling (ocean sampling, environmental monitoring) as Q -Learning problems leads to low-rank structures in the Q matrix (Ong, 2015; Yang et al., 2020b; Shah et al., 2020). Since these systems naturally consist of a large number of states, efficient exploitation of low rank structure of the Q matrix can potentially lead to significant reduction in computational complexity and improved performance. However, when the state space is high-dimensional and further, the state transition is probabilistic, high computational complexity of calculating the expectation of Q values of next states renders existing Q -Learning methods impractical.

A potential solution for this problem lies in approximating the expectation of Q values of next states with the sample mean of Q values over a subset of next states. A natural way to select a subset of next states is by drawing IID samples from the transition probability distribution. However, this straight forward approach becomes challenging when the state transition probability distribution is high-dimensional. This is because for IID sampling to be meaningful, the number of samples required to accurately approximate the expectation rapidly increase with the number of dimensions. We address this problem by sampling next states using Hamilton Monte Carlo. HMC method draws correlated samples from the region that maximizes the product of probability mass and volume thus leading to a better approximation of the expectation with a limited number of samples. In addition, using matrix completion methods to exploit the low rank structure of a Q matrix enables further improvement in data efficiency.

RELATED WORK

Data efficient Reinforcement Learning: The last decade has witnessed a significant interest in exploiting emergent global structures from underlying system dynamics for improving data efficiency in RL methods by. Deisenroth & Rasmussen (2011); Pan & Theodorou (2014); Kamthe & Deisenroth (2018); Buckman et al. (2018) have proposed model-based RL methods that improve data efficiency by explicitly incorporating prior knowledge about state transition dynamics of the underlying system. On the other hand, Ong (2015); Yang et al. (2020b) consider a model-free RL approach that exploit structures of state-action value function. The work by Ong (2015) considers decomposing the Q matrix to a low-rank and sparse matrix model and using matrix completion methods (Candes & Plan, 2010; Wen et al., 2012; Chen & Chi, 2018) to improve data efficiency. A more recent work by Yang et al. (2020b) adopts a similar approach and shows that by incorporating low rank matrix completion methods to complete partially updated Q matrix leads to improved performance. At each time step the agent chooses a subset of state-action pairs and update their Q value according to the Bellman optimally equation that considers a discounted average between reward and expectation of the Q values of next states. Shah et al. (2020) extends this work by proposing a novel matrix estimation method and providing theoretical guarantees for the convergence to a ϵ -optimal Q function. Lee et al. (2019) proposes an approach that samples a whole episode and then updates values in a recursive, backward manner.

CONTRIBUTION

The main contribution of this work is three-fold. *First*, we introduce a modified Q -learning framework, called Hamiltonian Q -learning, which uses HMC sampling for efficient computation of Q values. This innovation, by proposing to sample Q values from the region with the dominant contribution to the expectation of discounted reward, provides a data-efficient approach for using Q -learning in real-world problems with high-dimensional state space and probabilistic state transition. Furthermore, integration of this sampling approach with matrix-completion enables us to update Q values for only a small subset of state-action pairs and thereafter reconstruct the complete Q matrix. *Second*, we provide theoretical guarantees that the error between the optimal Q function and the Q function obtained by updating Q values using HMC sampling can be made arbitrarily small. This result also holds when only a handful of Q values are updated using HMC and the rest are estimated using matrix completion. *Finally*, we demonstrate the effectiveness of Hamiltonian Q -learning by applying it to a cart-pole stabilization problem and an adaptive ocean sampling problem. Our results also indicate that our proposed approach becomes more effective with increase in state space dimension.

2 PRELIMINARY CONCEPTS

In this section, we provide a brief background on Q -Learning, HMC sampling and matrix completion, as well as define the mathematical notations. In this paper, $|\mathcal{Z}|$ denotes the cardinality of a set \mathcal{Z} . Moreover, \mathbb{R} represent the real line and A^T denotes the transpose of matrix A .

2.1 Q -LEARNING

Markov Decision Process (MDP) is a mathematical formulation that captures salient features of sequential decision making (Bertsekas, 1995). In particular, a *finite MDP* is defined by the tuple $(\mathcal{S}, \mathcal{A}, \mathbb{P}, r, \gamma)$, where \mathcal{S} is the finite set of system states, \mathcal{A} is the finite set of actions, $\mathbb{P} : \mathcal{S} \times \mathcal{A} \times \mathcal{S} \rightarrow [0, 1]$ is the transition probability kernel, $r : \mathcal{S} \times \mathcal{A} \rightarrow \mathbb{R}$ is a bounded reward function, and $\gamma \in [0, 1)$ is a discounting factor. Without loss of generality, a state $s \in \mathcal{S}$ can be assumed to be a \mathcal{D}_s -dimensional real vector and an action $a \in \mathcal{A}$ can be assumed to be a \mathcal{D}_a -dimensional real vector. Moreover, by letting s^i denote the i th element of a state vector, we define the range of state space in terms of the following intervals $[d_i^-, d_i^+]$ such that $s^i \in [d_i^-, d_i^+]$ $\forall i \in \{1, \dots, \mathcal{D}_s\}$. At each time $t \in \{1, \dots, T\}$ over the time horizon of the decision making, the agent observes the state of the environment $s_t \in \mathcal{S}$ and takes an action a_t according to some policy π which maximizes the discounted cumulative reward. Once this action has been executed, the agent receives a reward $r(s_t, a_t)$ from the environment and the state of the environment changes to s_{t+1} . This state transition is governed by the transition probability kernel $\mathbb{P}(\cdot | s_t, a_t)$.

The Q function is a mapping from the space of state-action pairs to the real line, i.e. $Q : \mathcal{S} \times \mathcal{A} \rightarrow \mathbb{R}$, and it represents the expected discounted reward for taking a specific action at the current time and following the policy thereafter. Then by letting Q^t represent the Q matrix at time t , i.e. the tabulation of Q function over all possible state-action pairs associated with the finite MDP, we can express the Q value iteration over time steps as

$$Q^{t+1}(s_t, a_t) = \sum_{s \in \mathcal{S}} \mathbb{P}(s | s_t, a_t) \left(r(s_t, a_t) + \gamma \max_a Q^t(s, a) \right), \quad (1)$$

where \mathbb{E} denotes the expectation over the probability measure \mathbb{P} . Under this update rule (1), the Q function converges to the unique optimal value Q^* (Melo, 2001).

2.2 HAMILTONIAN MONTE CARLO

Hamiltonian Monte Carlo, an approach for drawing samples from probability distributions known up to a constant, offers faster convergence than Markov Chain Monte Carlo (MCMC) sampling (Neal et al., 2011; Betancourt; Betancourt et al., 2017; Neklyudov et al., 2020). We consider a smooth target distribution $\mathcal{P}(s)$ which is defined on the Euclidean space and

assumed to be analytically known up to a constant. HMC extends this target distribution to a joint distribution over a position variable (which is same as the target variable s) and an auxiliary momentum variable (v). Next, by exploiting the identity $\mathcal{P}(s, v) = \mathcal{P}(s)\mathcal{P}(v|s)$, we define the potential energy of the corresponding Hamiltonian as $U(s) = -\log \mathcal{P}(s)$ and the kinetic energy as $K(v, s) = -\log \mathcal{P}(v|s) = \frac{1}{2}v^T M^{-1}v$ for a suitable choice of mass matrix M . Then the Hamiltonian of the system can be expressed as

$$H(s, v) = -\log \mathcal{P}(s, v) = U(s) + K(v, s).$$

HMC sampling method consists of two main steps - in the *first step*, a new momentum variable v is drawn from a fixed probability distribution, typically a multivariate Gaussian; and in the *second step*, a new proposal (s', v') is obtained by generating a trajectory that starts from (s, v) and obeys Hamilton dynamics. Following the Metropolis–Hastings acceptance/rejection rule, this new proposal is accepted with probability

$$\min \left\{ 1, \frac{\exp(H(s, v))}{\exp(H(s', -v'))} \right\}.$$

We integrate the Hamiltonian dynamics for L steps with step size Δl to generate the trajectory from (s, v) to (s', v') . To ensure that the Hamiltonian is conserved along the trajectory, we use a volume preserving symplectic integrator, in particular a leapfrog integrator which uses the following update rule to go from step l to $l + \Delta l$:

$$v_{l+\frac{\Delta l}{2}} = v_l - 0.5\Delta l \partial_s U(s_l); \quad s_{l+\Delta l} = s_l + \Delta l M^{-1} v_{l+\frac{\Delta l}{2}}; \quad v_{l+\Delta l} = v_l - 0.5\Delta l \partial_s U(s_{l+\Delta l}).$$

2.3 MATRIX COMPLETION

Matrix completion focuses on recovering a matrix $X \in \mathbb{R}^{n \times m}$ by observing only a small fraction of its individual elements (Xu et al., 2013; Chen & Chi, 2018). To estimate a reconstruction $Z \in \mathbb{R}^{n \times m}$ of the matrix X , matrix completion algorithms minimize the error between X and Z with respect to some appropriate matrix norm. Often this approach focuses on recovering low rank and sparse matrix structures which can be interpreted as a constraint on the nuclear norm of the reconstructed matrix, i.e., the sum of its singular values. Therefore, matrix completion can be expressed as

$$Z = \arg \min_{Y \in \mathbb{R}^{n \times m}} \|Y\|_* \quad \text{subject to} \quad \mathcal{J}_\Omega(Y) = \mathcal{J}_\Omega(X) \quad (2)$$

where $\|\cdot\|_*$ denotes the nuclear norm, Ω is the observed set of elements, and \mathcal{J}_Ω is the observation operator, i.e. $\mathcal{J}_\Omega(x) = x$ if $x \in \Omega$ and zero otherwise.

3 HAMILTONIAN Q -LEARNING

A large class of real world sequential decision making problems - for example, board/video games, control of robots' movement, and portfolio optimization - involves high-dimensional state spaces and often has large number of distinct states along each individual dimension. As using a Q -Learning based approach to train RL-agents for these problems typically requires tens to hundreds of millions of samples (Mnih et al., 2015; Silver et al., 2017), there is a strong need for data efficient algorithms for Q -Learning. In addition, state transition in such systems is often probabilistic in nature; even when the underlying dynamics of the system is inherently deterministic; presence of external disturbances and parameter variations/uncertainties lead to probabilistic state transitions.

Learning an optimal Q^* function through value iteration methods requires updating Q values of state-action pairs using a sum of the reward and a discounted expectation of Q values associated with next states. In this work, we assume the reward to be a deterministic function of state-action pairs. However, when the reward is stochastic, these results can be extended by replacing the reward with its expectation. Subsequently, we can express (1) as

$$Q^{t+1}(s_t, a_t) = r(s_t, a_t) + \gamma \mathbb{E} \left(\max_a Q^t(s, a) \right). \quad (3)$$

When the underlying state space is high-dimensional and has large number of states, obtaining a more accurate estimate of the expectation is computationally very expensive. The complexity increases quadratically with the number of states and linearly with number of actions, rendering the existing algorithms impractical. In this work, we propose a solution to this issue by introducing an importance-sampling based method to approximate the aforementioned expectation.

A Naive Solution and Its Limitations: Approximating the expectation by a sample mean of Q values over a subset of next states provides a potential solution to this problem. A natural way to sample a subset from the set of all possible next states is to draw identically and independently distributed (IID) samples from the transition probability distribution $\mathbb{P}(\cdot|s_t, a_t)$. However, when the transition probability is defined over a high-dimensional space, this naive solution fails.

With increase in state dimension, the volume fraction that lies away from the high probability density region in the state space also increases. This is illustrated in the first row of Figure 1. However, a dominant contribution to the expectation comes from the region that maximizes the probability mass, i.e., the product of probability density and volume provides. As illustrated in the second row of Figure 1, most of samples in a limited pool of IID samples concentrate around the region with high probability density. Consequently, IID sampling provides a poor approximation for the expectation.

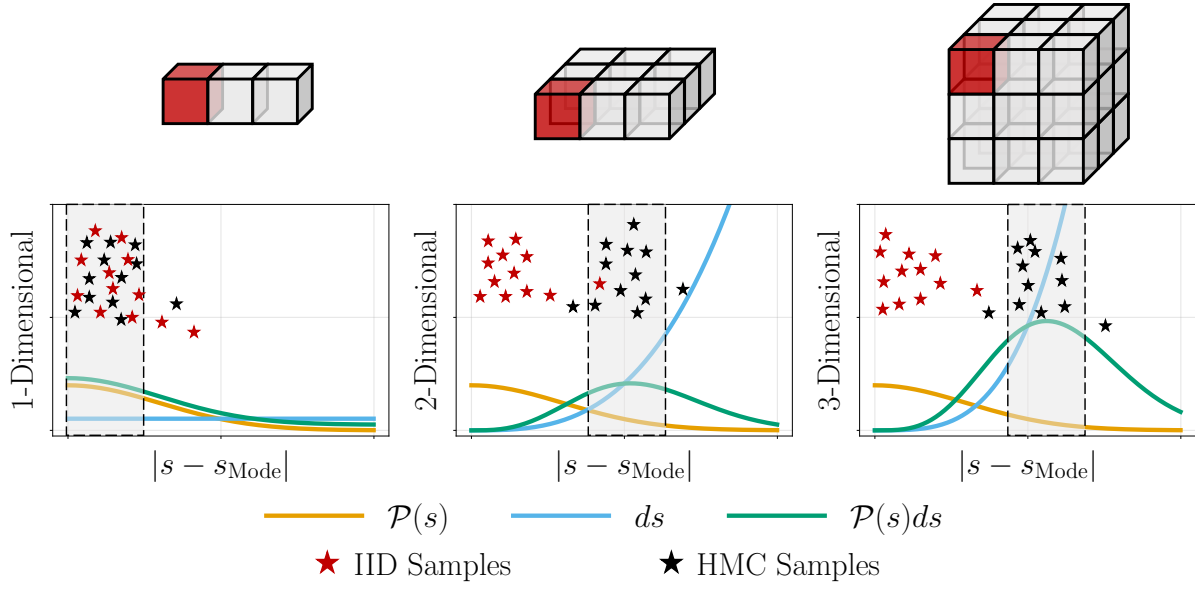


Figure 1: The first row illustrates that, as the dimension of the space increases, the relative volume inside a partition compared to the volume outside of the partition decreases. When the dimension increases from 1 through 3, the relative volume of red partition decreases as 1, 1/9 and 1/27, respectively. The second row shows how the region over which IID samples and HMC samples are concentrated varies with increase in dimension of the probability space. Here $\mathcal{P}(s)$, s_{Mode} and ds represent probability density, mode of the distribution and volume, respectively. Note that IID samples concentrate in the region with high probability density (orange curve), i.e., around the mode. As dimension increases a larger volume lies away from the mode (blue curve). Contribution to the expectation is determined by the probability mass (green curve), i.e., product of probability density and volume. HMC samples are concentrated in the region that maximizes probability mass (grey area).

3.1 DATA EFFICIENCY THROUGH HMC SAMPLING

A number of importance-sampling methods (Liu, 1996; Betancourt) have been developed for estimating the expectation of a function by drawing samples from the region with the dominant contribution to the expectation. HMC is one such importance-sampling method that draws samples from the typical set, i.e., the region that maximizes probability mass, which provides the dominated contribution to the expectation. As shown in the second row of Figure 1, most of the samples in a limited pool of HMC samples indeed concentrate around the region with high probability mass. Since the decay in Q function is significantly smaller compared to the typical exponential or power law decays in transition probability function, HMC provides a better approximation for the expectation of the Q value of the next states (Yang et al., 2020b; Shah et al., 2020). Then by letting \mathcal{H}_t denote the set of HMC samples drawn at time step t , we update the Q values as:

$$Q^{t+1}(s_t, a_t) = r(s_t, a_t) + \frac{\gamma}{|\mathcal{H}_t|} \sum_{s \in \mathcal{H}_t} \max_a Q^t(s, a). \quad (4)$$

HMC for a smooth truncated target distribution: Recall that region of states is a subset of a Euclidean space given as $s \in [d_1^-, d_1^+] \times \dots \times [d_{\mathcal{D}_s}^-, d_{\mathcal{D}_s}^+] \subset \mathbb{R}^{\mathcal{D}_s}$. Thus the main challenge to using HMC sampling is to define a smooth continuous target distribution $\mathcal{P}(s|s_t, a_t)$ which is defined on $\mathbb{R}^{\mathcal{D}_s}$ with a sharp decay at the boundary of the region of states (Yi & Doshi-Velez, 2017; Chevallier et al., 2018). In this work, we generate the target distribution by first defining the transition probability kernel from the conditional probability distribution defined on $\mathbb{R}^{\mathcal{D}_s}$ and then multiplying it with a smooth cut-off function.

We first consider a probability distribution $\mathcal{P}(\cdot|s_t, a_t) : \mathbb{R}^{\mathcal{D}_s} \rightarrow \mathbb{R}$ such that the following holds

$$\mathbb{P}(s|s_t, a_t) \propto \int_{s-\varepsilon}^{s+\varepsilon} \mathcal{P}(s|s_t, a_t) ds \quad (5)$$

for some arbitrarily small $\varepsilon > 0$. Then the target distribution can be defined as

$$\mathcal{P}(s|s_t, a_t) = \mathcal{P}(s|s_t, a_t) \prod_{i=1}^{\mathcal{D}_s} \frac{1}{1 + \exp(-\kappa(d_i^+ - s^i))} \frac{1}{1 + \exp(-\kappa(s^i - d_i^-))}. \quad (6)$$

Note that there exists a large $\kappa > 0$ such that if $s \in [d_1^-, d_1^+] \times \dots \times [d_{\mathcal{D}_s}^-, d_{\mathcal{D}_s}^+]$ then $\mathcal{P}(s|s_t, a_t) \propto \mathbb{P}(s|s_t, a_t)$ and $\mathcal{P}(s|s_t, a_t) \approx 0$ otherwise. Let $\mu(s_t, a_t)$, $\Sigma(s_t, a_t)$ be the mean vector and covariance matrix of the transition probability kernel. In this paper we consider transition probability kernels of the form

$$\mathbb{P}(s|s_t, a_t) \propto \exp\left(-\frac{1}{2}(s - \mu(s_t, a_t))^T \Sigma^{-1}(s_t, a_t)(s - \mu(s_t, a_t))\right). \quad (7)$$

Then from (5) the corresponding mapping can be given as a multivariate Gaussian $\mathcal{P}(s|s_t, a_t) = \mathcal{N}(\mu(s_t, a_t), \Sigma(s_t, a_t))$. Thus from (6) it follows that the target distribution is

$$\mathcal{P}(s|s_t, a_t) = \mathcal{N}(\mu(s_t, a_t), \Sigma(s_t, a_t)) \prod_{i=1}^{\mathcal{D}_s} \frac{1}{1 + \exp(-\kappa(d_i^+ - s^i))} \frac{1}{1 + \exp(-\kappa(s^i - d_i^-))} \quad (8)$$

Choice of kinetic energy and mass matrix: Recall that the target distribution $\mathcal{P}(s|s_t, a_t)$ is defined over the Euclidean space $\mathbb{R}^{\mathcal{D}_s}$. For brevity of notation we drop the explicit dependence on (s_t, a_t) and denote the target distribution as $\mathcal{P}(s)$. First we consider an Euclidean metric \mathcal{M} that induces the distance between \tilde{s}, \bar{s} as $d(\tilde{s}, \bar{s}) = (\tilde{s} - \bar{s})^T \mathcal{M}(\tilde{s} - \bar{s})$. Then we define $\mathcal{M}_s \in \mathbb{R}^{\mathcal{D}_s \times \mathcal{D}_s}$ as a diagonal scaling matrix and $\mathcal{M}_r \in \mathbb{R}^{\mathcal{D}_s \times \mathcal{D}_s}$ as a rotation matrix in dimension \mathcal{D}_s . With this we can define M as $M = \mathcal{M}_r \mathcal{M}_s \mathcal{M}_r^T$. Thus, any metric M that defines an Euclidean structure on the target variable space induces an inverse structure on the momentum variable space as $d(\tilde{v}, \bar{v}) = (\tilde{v} - \bar{v})^T M^{-1}(\tilde{v} - \bar{v})$. This generates a natural family of multivariate Gaussian distributions such that $\mathcal{P}(v|s) = \mathcal{N}(0, M)$ leading to the kinetic energy $K(v, s) = -\log \mathcal{P}(v|s) = v^T M^{-1} v$.

3.2 Q-LEARNING WITH HMC AND MATRIX COMPLETION

In this work we consider problems with a high-dimensional state space and large number of distinct states along individual dimensions. Since the size of Q matrix is $|\mathcal{S}| \times |\mathcal{A}|$, these problems admit a large Q matrix. However, as the underlying system dynamics often lead to a low rank structure, we can further improve the data efficiency by exploiting the low rank structure of the Q matrix.

At each time step t we randomly sample a subset Ω_t of state-action pairs (each state-action pair is sampled independently with some probability p) and update the Q function for state-action pairs in Ω_t . Let \hat{Q}^{t+1} be the updated Q matrix at time t . Then from (4) we have

$$\hat{Q}^{t+1}(s_t, a_t) = r(s_t, a_t) + \frac{\gamma}{|\mathcal{H}_t|} \sum_{s \in \mathcal{H}_t} \max_a Q^t(s, a), \quad \forall (s_t, a_t) \in \Omega_t. \quad (9)$$

Then we recover the complete matrix Q^{t+1} by using the method given in (2). Thus we have

$$Q^{t+1} = \arg \min_{\tilde{Q}^{t+1} \in \mathbb{R}^{|\mathcal{S}| \times |\mathcal{A}|}} \|\tilde{Q}^{t+1}\|_* \quad \text{subject to} \quad \mathcal{J}_{\Omega_t}(\tilde{Q}^{t+1}) = \mathcal{J}_{\Omega_t}(\hat{Q}^{t+1}). \quad (10)$$

Taking a similar approach to the one presented in (Yang et al., 2020b), we approximate the rank of the Q matrix as the minimum number of singular values that are needed to capture 99% of its nuclear norm.

Algorithm 1 Hamiltonian Q-Learning

Inputs: Discount factor γ ; Range of state space; Time horizon T ;

Initialization: Randomly initialize Q^0

for $t = 1$ **to** T **do**

Step 1: Randomly sample a subset of state-action pairs Ω :

Step 2: **HMC sampling phase** Sample a set of next states \mathcal{H}_t according to the target distribution defined in (6) :

Step 3: **Update phase** For all $(s_t, a_t) \in \Omega_t$

$$\hat{Q}^{t+1}(s_t, a_t) = r(s_t, a_t) + \frac{\gamma}{|\mathcal{H}_t|} \sum_{s \in \mathcal{H}_t} \max_a Q^t(s, a)$$

Step 4: **Matrix Completion phase**

$$Q^{t+1} = \arg \min_{\tilde{Q}^{t+1} \in \mathbb{R}^{|\mathcal{S}| \times |\mathcal{A}|}} \|\tilde{Q}^{t+1}\|_* \quad \text{subject to} \quad \mathcal{J}_{\Omega_t}(\tilde{Q}^{t+1}) = \mathcal{J}_{\Omega_t}(\hat{Q}^{t+1})$$

end for

3.3 CONVERGENCE AND BOUNDEDNESS GUARANTEES

In this section we provide main theoretical results of the paper. Let $n_{\mathcal{H}} = \min_{\tau} |\mathcal{H}_{\tau}|$.

Definition 1 (ϵ optimal Q functions). Let Q^* be the unique fixed point of the Bellman optimality equation given as $(\mathcal{T}Q)(s', a') = \sum_{s \in \mathcal{S}} \mathbb{P}(s|s', a') (r(s', a') + \gamma \max_a Q(s, a))$, $\forall (s', a') \in \mathcal{S} \times \mathcal{A}$ where \mathcal{T} is the Bellman operator. Then, under update rule (3), the Q function almost surely converges to the optimal Q^* . We define ϵ optimal Q functions as the family of functions \mathbf{Q}_{ϵ} such that $\|Q' - Q^*\|_{\infty} \leq \epsilon$ whenever $Q' \in \mathbf{Q}_{\epsilon}$.

Theorem 1. (Convergence of Q function under HMC) Let \mathcal{T} be an optimality operator under HMC given as $(\mathcal{T}Q)(s', a') = r(s', a') + \frac{\gamma}{|\mathcal{H}|} \sum_{s \in \mathcal{H}} \max_a Q(s, a)$, $\forall (s', a') \in \mathcal{S} \times \mathcal{A}$, where \mathcal{H} is a subset of next states sampled using HMC from the target distribution given in (6). Then, under update rule (4) and for any given $\epsilon \geq 0$, there exists $n_{\mathcal{H}}, t' > 0$ such that $\|Q^t - Q^*\|_{\infty} \leq \epsilon \forall t \geq t'$.

Theorem 1 states that the Q function converges to the space of ϵ optimal Q functions under update rule (4). Its proof is given in Appendix A.1.

Theorem 2. (Boundedness of Q function under matrix completion) Let $Q_{\varepsilon}^{t+1}(s_t, a_t) = r(s_t, a_t) + \gamma \sum_{s \in \mathcal{S}} \mathbb{P}(s|s_t, a_t) \max_a Q_{\varepsilon}^t(s, a), \forall (s_t, a_t) \in \mathcal{S} \times \mathcal{A}$ be the update rule under exhaustive sampling, and Q^t be the Q function updated according to Hamiltonian Q -Learning, i.e. by (9)-(10). Then, for any given $\tilde{\varepsilon} \geq 0$, there exists $n_{\mathcal{H}}, t' > 0$, such that $\|Q^t - Q_{\varepsilon}^t\|_{\infty} \leq \tilde{\varepsilon} \forall t \geq t'$.

Theorem 2 states that under matrix completion Q function is bounded. Its proof is given in Appendix A.2.

3.4 EMPIRICAL EVALUATION FOR CART-POLE

Experimental setup: We consider a cart-pole system. By letting $\theta, \dot{\theta}$ denote the angle and angular velocity of the pole and x, \dot{x} denote the position and velocity of the cart, the 4-dimensional state vector for this system can be defined as $s = (\theta, \dot{\theta}, x, \dot{x})$. After defining the range of state space as $\theta \in [-\pi/2, \pi/2]$, $\dot{\theta} \in [-3.0, 3.0]$, $x \in [-2.4, 2.4]$ and $\dot{x} \in [-3.5, 3.5]$, we define the range of the scalar action as $a \in [-10, 10]$. Then each state space dimension is discretized into 5 distinct values and the action space into 10 distinct values. This forms a Q matrix of size 625×10 . To capture parameter uncertainties and external disturbances, we assume that the probabilistic state transition is governed by a multivariate Gaussian with zero mean and covariance $\Sigma = \text{diag}[0.143, 0.990, 0.635, 1.346]$. To drive the pole to an upright position, we define the reward function as $r(s, a) = \cos^4(15\theta)$ (Yang et al., 2020b). After initializing the Q matrix using randomly chosen values from $[0, 1]$, we sample state-action pairs independently with probability $p = 0.5$ at each iteration. Additional experimental details and results are provided in Appendix B.

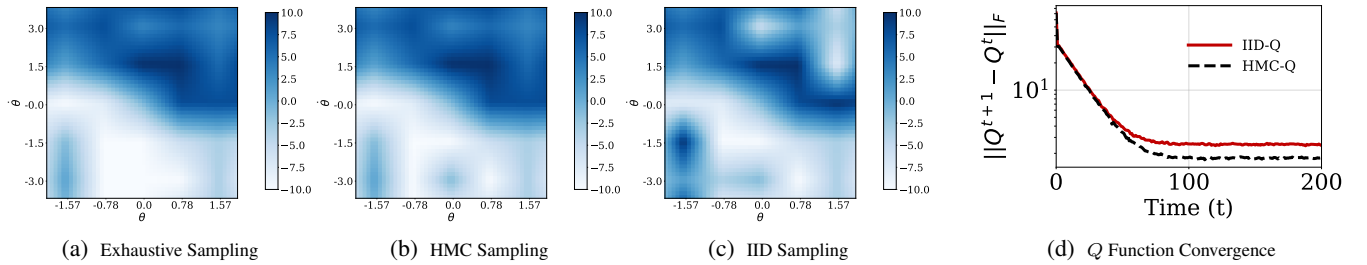


Figure 2: Figure 2(a), 2(b) and 2(c) show policy heat maps for Q -Learning with exhaustive sampling, Hamiltonian Q -Learning and Q -Learning with IID sampling, respectively. Figure 2(d) provides a comparison for convergence of Q function with Hamiltonian Q -Learning and Q -Learning with IID sampling.

Results: As it is difficult to visualize a heat map for a 4-dimensional state space, we show results for the first two dimensions $\theta, \dot{\theta}$ with fixed x, \dot{x} . The color in each cell of the heat maps shown in Figures 2(a), 2(b) and 2(c) indicates the value of optimal action associated with that state. These figures illustrate that the policy heat map for Hamiltonian Q -Learning is closer to the policy heat map for Q -Learning with exhaustive sampling. The two curves in Figure 2(d), that show the Frobenius norm of the difference between Q function values from consecutive time steps, illustrate that Hamiltonian Q -Learning achieves better convergence than Q -Learning with IID sampling.

4 APPLICATION TO OCEAN SAMPLING

Ocean sampling plays a major role in a variety of science and engineering problems, ranging from modeling marine ecosystems to predicting global climate. Here, we consider the problem of using an under water glider to obtain measurements of a scalar field (e.g., temperature, salinity or concentration of a certain zooplankton) and illustrate how the use of Hamiltonian Q -Learning in planning the glider trajectory can lead to measurements that minimize the uncertainty associated with the field.

4.1 FORMULATION AS A MDP

States, actions and state transition: By assuming that the glider’s motion is restricted to an horizontal plane (Refael & Degani, 2019), we let x, y and θ denote its center of mass position and heading angle, respectively. Then we can define the 6-dimensional state vector for this system as $s = (x, y, \dot{x}, \dot{y}, \theta, \dot{\theta})$ and the action a as a scalar control input to the glider. Also, to accommodate dynamic perturbations due to the ocean current, other external disturbances and parameter uncertainties, we assume that the probabilistic state transition is governed by a multivariate Gaussian.

Reward: As ocean fields often exhibit temporal and spatial correlations (Leonard et al., 2007), this work focuses on spatially correlated scalar fields. Following the approach of Leonard et al. (2007), we define ocean statistic correlation between two positions \mathbf{q} and \mathbf{q}' as $B(\mathbf{q}, \mathbf{q}') = \exp(-\|\mathbf{q} - \mathbf{q}'\|^2/\sigma^2)$, where σ is the spatial decorrelation scale. The goal of the task is to take measurements that reduce the uncertainty associated with the field. Now we assume that the glider takes N measurements at positions $\mathbf{q}_1, \dots, \mathbf{q}_N$. Then covariance of the collected data set can be given by a $N \times N$ matrix \mathcal{W} such that its i th row and the j th column element is: $\mathcal{W}_{ij} = \eta\delta_{ij} + B(\mathbf{q}_i, \mathbf{q}_j)$, where δ_{ij} is the Dirac delta and η is the variance of the uniform and uncorrelated measurement noise. Then using objective analysis data assimilation scheme (Kalnay, 2003; Bennett, 2005), the

total reduction of uncertainty of the field after the measurements can be expressed as

$$\mathcal{U} = \sum_{\mathbf{q} \in \mathcal{Q}} \sum_{i,j=1}^N B(\mathbf{q}, \mathbf{q}_i) \mathcal{W}_{ij}^{-1} B(\mathbf{q}_j, \mathbf{q}), \quad (11)$$

where \mathcal{Q} is the set of all position variables. By substituting the formulas from (Kalnay, 2003; Bennett, 2005) into (11), this formulation can be generalized to Gaussian measurement noise.

Note that $\arg \max_{s'} \mathbb{P}(s'|s, a)$ is the maximally probable next state for the state-action pair (s, a) . Let \mathcal{Z}_s be the set that contains state s and its maximally probable next states for all actions. Recall that $s = (x, y, \dot{x}, \dot{y}, \theta, \dot{\theta}) = (\mathbf{q}, \dot{\mathbf{q}}, \theta, \dot{\theta})$. Now we proceed to define the reward function as follows. Without loss of generality, we assume that the glider is deployed from $\mathbf{q} = (0, 0)$ and retrieving the glider incurs a cost depending on its position. Then we introduce a reward that aims to reduce uncertainty of the scalar field while penalizing the movements away from the origin, and define it as

$$r(s, a) = -\lambda \mathbf{q}^T \mathcal{C} \mathbf{q} + \sum_{\mathbf{q} \in \mathcal{Q}} \sum_{i,j \in \mathcal{Z}_s} B(\mathbf{q}, \mathbf{q}_i) \mathcal{W}_{ij}^{-1} B(\mathbf{q}_j, \mathbf{q}),$$

where $\lambda > 0$ maintains a balance between the two objectives and $\mathcal{C} = \mathcal{C}^T \geq 0$.

4.2 EMPIRICAL EVALUATION

Experimental setup We define the range of state and action space as $x, y \in [-10, 10]$, $\dot{x}, \dot{y} \in [-25, 25]$, $\theta \in [-\pi, \pi]$, $\dot{\theta} \in [-3, 3]$, and $a \in [-1, 1]$, respectively and then discretizing each state dimension into 5 distinct values and the action space into 5 distinct values, we have a Q matrix of size 15625×5 . Also, we assume that the state transition kernel is given by a multivariate Gaussian with zero mean and covariance $\Sigma = \text{diag}[11.111, 69.444, 11.111, 69.444, 0.143, 0.990]$. After initializing the Q matrix using randomly chosen values from $[0, 1]$, we sample state-action pairs independently with probability $p = 0.5$ at each iteration. Also, we assume $\sigma = 2.5$, $\lambda = 0.1$, $\mathcal{C} = \text{diag}[1, 0]$. Additional experimental details and results are provided in Appendix C

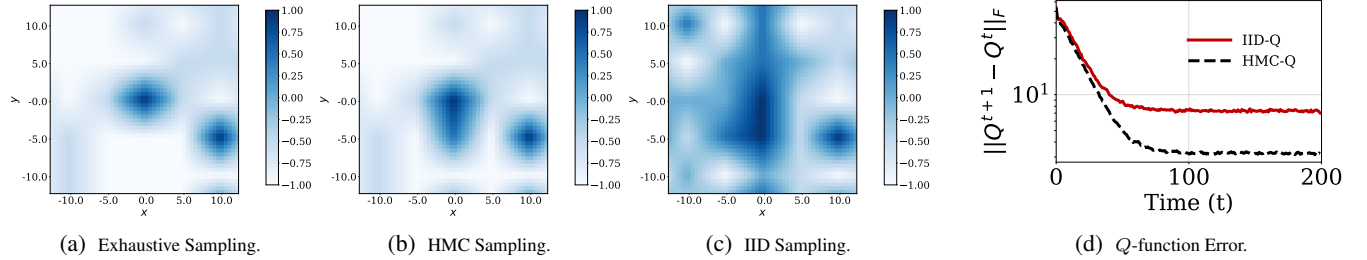


Figure 3: Figure 3(a), 3(b) and 3(c) show policy heat maps for Q -Learning with exhaustive sampling, Hamiltonian Q -Learning and Q -Learning with IID sampling respectively. Figure 3(d) provides a comparison for convergence of Q function with Hamiltonian Q -Learning and Q -Learning with IID sampling.

Results Figures 3(a), 3(b) and 3(c) show the policy heat map over first two dimensions x, y with fixed \dot{x}, \dot{y}, θ and $\dot{\theta}$. The color of each cell indicates the value of optimal action associated with that state. These figures illustrate that the difference between policy heat maps associated with Hamiltonian Q -Learning and Q -Learning with exhaustive sampling is smaller than the difference between policy heat maps associated with Q -Learning with IID sampling and Q -Learning with exhaustive sampling. The two curves in Figure 3(d), that show the Frobenius norm of the difference between Q function values from consecutive time steps, illustrate that Hamiltonian Q -Learning achieves better convergence than Q -Learning with IID sampling. A comparison between results of the ocean sampling problem and the cart-pole stabilization problem indicates that Hamiltonian Q -Learning provides increasingly better performance with increase in state space dimension.

5 CONCLUSION

Here we have introduced *Hamiltonian Q -Learning* which utilizes HMC sampling with matrix completion methods to improve data efficiency. We show, both theoretically and empirically, that the proposed approach can learn very accurate estimates of the optimal Q function with much fewer data points. We also demonstrate that Hamiltonian Q -Learning performs significantly better than Q -Learning with IID sampling when the underlying state space dimension is large. By building upon this aspect, future works will investigate how importance-sampling based methods can improve data-efficiency in multi-agent Q -learning with agents coupled through both action and reward.

REFERENCES

- Andrew F Bennett. *Inverse modeling of the ocean and atmosphere*. Cambridge University Press, 2005.
- Dimitri P Bertsekas. *Dynamic Programming and Optimal Control*, volume 1. Athena Scientific Belmont, MA, 1995.

- Michael Betancourt. A conceptual introduction to Hamiltonian Monte Carlo.
- Michael Betancourt, Simon Byrne, Sam Livingstone, Mark Girolami, et al. The geometric foundations of Hamiltonian Monte Carlo. *Bernoulli*, 23(4A):2257–2298, 2017.
- Jacob Buckman, Danijar Hafner, George Tucker, Eugene Brevdo, and Honglak Lee. Sample-efficient reinforcement learning with stochastic ensemble value expansion. In *Advances in Neural Information Processing Systems*, pp. 8224–8234, 2018.
- Emmanuel J Candes and Yaniv Plan. Matrix completion with noise. *Proceedings of the IEEE*, 98(6):925–936, 2010.
- Yudong Chen and Yuejie Chi. Harnessing structures in big data via guaranteed low-rank matrix estimation: Recent theory and fast algorithms via convex and nonconvex optimization. *IEEE Signal Processing Magazine*, 35(4):14–31, 2018.
- Augustin Chevallier, Sylvain Pion, and Frédéric Cazals. Hamiltonian Monte Carlo with boundary reflections, and application to polytope volume calculations. 2018.
- Marc Deisenroth and Carl E Rasmussen. Pilco: A model-based and data-efficient approach to policy search. In *International Conference on Machine Learning (ICML)*, pp. 465–472, 2011.
- Yan Duan, Xi Chen, Rein Houthoofd, John Schulman, and Pieter Abbeel. Benchmarking deep reinforcement learning for continuous control. In *International Conference on Machine Learning (ICML)*, pp. 1329–1338, 2016.
- Susan Holmes, Simon Rubinstein-Salzedo, and Christof Seiler. Curvature and concentration of Hamiltonian Monte Carlo in high dimensions. *arXiv:1407.1114*, 2014.
- Eugenia Kalnay. *Atmospheric modeling, data assimilation and predictability*. Cambridge University Press, 2003.
- Sanket Kamthe and Marc Deisenroth. Data-efficient reinforcement learning with probabilistic model predictive control. In *International Conference on Artificial Intelligence and Statistics*, pp. 1701–1710. PMLR, 2018.
- Jens Kober, J Andrew Bagnell, and Jan Peters. Reinforcement learning in robotics: A survey. *The International Journal of Robotics Research*, 32(11):1238–1274, 2013.
- Su Young Lee, Choi Sungik, and Sae-Young Chung. Sample-efficient deep reinforcement learning via episodic backward update. In *Advances in Neural Information Processing Systems*, pp. 2112–2121, 2019.
- Naomi E. Leonard, Derek A. Paley, Francois Lekien, Rodolphe Sepulchre, David M. Fratantoni, and Russ E. Davis. Collective motion, sensor networks, and ocean sampling. *Proceedings of the IEEE*, 95(1):48–74, 2007.
- Jun S Liu. Metropolized independent sampling with comparisons to rejection sampling and importance sampling. *Statistics and Computing*, 6(2):113–119, 1996.
- DHS Maithripala, TWU Madhushani, and JM Berg. A Geometric PID Control Framework for Mechanical Systems. *arXiv:1610.04395*, 2016.
- Hongzi Mao, Mohammad Alizadeh, Ishai Menache, and Srikanth Kandula. Resource management with deep reinforcement learning. In *Proceedings of the 15th ACM Workshop on Hot Topics in Networks*, pp. 50–56, 2016.
- Rowan McAllister and Carl Edward Rasmussen. ta-efficient reinforcement learning in continuous state-action Gaussian-POMDPs. In *Advances in Neural Information Processing Systems*, pp. 2040–2049, 2017.
- Francisco S Melo. Convergence of Q-learning: A simple proof. *Institute Of Systems and Robotics, Tech. Rep*, pp. 1–4, 2001.
- Volodymyr Mnih, Koray Kavukcuoglu, David Silver, Andrei A Rusu, Joel Veness, Marc G Bellemare, Alex Graves, Martin Riedmiller, Andreas K Fidjeland, Georg Ostrovski, et al. Human-level control through deep reinforcement learning. *Nature*, 518(7540):529–533, 2015.
- Radford M Neal et al. MCMC using Hamiltonian dynamics. *Handbook of Markov Chain Monte Carlo*, 2(11):2, 2011.
- Kirill Neklyudov, Max Welling, Evgenii Egorov, and Dmitry Vetrov. Involutive MCMC: A Unifying Framework. *arXiv:2006.16653*, 2020.
- Hao Yi Ong. Value function approximation via low-rank models. *arXiv:1509.00061*, 2015.
- Yunpeng Pan and Evangelos Theodorou. Probabilistic differential dynamic programming. In *Advances in Neural Information Processing Systems*, pp. 1907–1915, 2014.
- Gilad Refael and Amir Degani. A single-actuated swimming robot: Design, modelling, and experiments. *Journal of Intelligent & Robotic Systems*, 94(2):471–489, 2019.

- Devavrat Shah, Dogyoon Song, Zhi Xu, and Yuzhe Yang. Sample efficient reinforcement learning via low-rank matrix estimation. *arXiv:2006.06135*, 2020.
- David Silver, Julian Schrittwieser, Karen Simonyan, Ioannis Antonoglou, Aja Huang, Arthur Guez, Thomas Hubert, Lucas Baker, Matthew Lai, Adrian Bolton, et al. Mastering the game of Go without human knowledge. *Nature*, 550(7676):354–359, 2017.
- Richard S Sutton and Andrew G Barto. *Reinforcement learning: An introduction*. MIT press, 2018.
- Christopher JCH Watkins. *Learning from delayed rewards*. PhD thesis, King’s College, Cambridge, Cambridge, UK, 1989.
- Christopher JCH Watkins and Peter Dayan. Q-learning. *Machine learning*, 8(3-4):279–292, 1992.
- Zaiwen Wen, Wotao Yin, and Yin Zhang. Solving a low-rank factorization model for matrix completion by a nonlinear successive over-relaxation algorithm. *Mathematical Programming Computation*, 4(4):333–361, 2012.
- Yangyang Xu, Ruru Hao, Wotao Yin, and Zhixun Su. Parallel matrix factorization for low-rank tensor completion. *arXiv:1312.1254*, 2013.
- Yuxiang Yang, Ken Caluwaerts, Atil Iscen, Tingnan Zhang, Jie Tan, and Vikas Sindhwani. Data efficient reinforcement learning for legged robots. In *Conference on Robot Learning*, pp. 1–10. PMLR, 2020a.
- Yuzhe Yang, Guo Zhang, Zhi Xu, and Dina Katabi. Harnessing structures for value-based planning and reinforcement learning. In *International Conference on Learning Representations (ICLR)*, 2020b.
- Kexin Yi and Finale Doshi-Velez. Roll-back Hamiltonian Monte Carlo. *arXiv:1709.02855*, 2017.
- Zhenpeng Zhou, Xiaocheng Li, and Richard N Zare. Optimizing chemical reactions with deep reinforcement learning. *ACS Central Science*, 3(12):1337–1344, 2017.

A CONVERGENCE AND BOUNDEDNESS RESULTS

We proceed to prove theorem by stating convergence properties for HMC as follows. In the initial sampling stage, starting from the initial position Markov chain converges towards to the typical set. In the next stage Markov chain quickly traverse the typical set and improves the estimate by removing the bias. In the last stage Markov chain refine the exploration of typical the typical set provide improved estimates. The number of samples taken during the last stage is referred as effective sample size.

A.1 PROOF OF THEOREM 1

Theorem 1. Let \mathcal{T} be an optimality operator under HMC given as $(\mathcal{T}Q)(s', a') = r(s', a') + \frac{\gamma}{|\mathcal{H}|} \sum_{s \in \mathcal{H}} \max_a Q(s, a)$, $\forall (s', a') \in \mathcal{S} \times \mathcal{A}$, where \mathcal{H} is a subset of next states sampled using HMC from the target distribution given in (6). Then, under update rule (4) and for any given $\epsilon \geq 0$, there exists $n_{\mathcal{H}}, t' > 0$ such that $\|Q^t - Q^*\|_{\infty} \leq \epsilon$ $\forall t \geq t'$.

Proof of Theorem 1. Let $\bar{Q}^t(s, a) = \frac{1}{n_{\mathcal{H}}} \max_a Q^t(s, a)$, $\forall (s, a) \in \mathcal{S} \times \mathcal{A}$. Here we consider $n_{\mathcal{H}}$ to be the effective number of samples. Let $\mathbb{E}_{\mathcal{P}} Q^t$, $\text{Var}_{\mathcal{P}} Q^t$ be the expectation and covariance of Q^t with respect to the target distribution. From Central Limit Theorem for HMC we have

$$\bar{Q}^t \sim \mathcal{N} \left(\mathbb{E}_{\mathcal{P}} Q^t, \sqrt{\frac{\text{Var}_{\mathcal{P}} Q^t}{n_{\mathcal{H}}}} \right).$$

Since Q function does not decay fast we provide a proof for the case where Q^t is C -Lipschitz. From Theorem 6.5 in (Holmes et al., 2014) we have that, there exists a $c_0 > 0$ such that

$$\|\bar{Q}^t - \mathbb{E}_{\mathcal{P}} Q^t\| \leq c_0. \quad (12)$$

Recall that Bellman optimality operator \mathcal{T} is a contraction mapping. Thus from triangle inequality we have

$$\begin{aligned} \|\mathcal{T}Q_1 - \mathcal{T}Q_2\|_{\infty} &\leq \max_{s', a'} \left\| r(s', a') + \frac{\gamma}{|\mathcal{H}_1|} \sum_{s \in \mathcal{S}} \max_a Q_1(s, a) \right. \\ &\quad \left. - r(s', a') - \frac{\gamma}{|\mathcal{H}_2|} \sum_{s \in \mathcal{S}} \max_a Q_2(s, a) \right\| \\ &\leq \max_{s', a'} \left\| \frac{\gamma}{|\mathcal{H}_1|} \sum_{s \in \mathcal{S}} \max_a Q_1(s, a) - \frac{\gamma}{|\mathcal{H}_2|} \sum_{s \in \mathcal{S}} \max_a Q_2(s, a) \right\| \end{aligned}$$

Let $|\mathcal{H}_1| = |\mathcal{H}_2| = n_{\mathcal{H}}$. Then using triangle inequality we have

$$\|\mathcal{T}Q_1 - \mathcal{T}Q_2\|_{\infty} \leq \max_{s', a'} \gamma \left[\|\bar{Q}_1 - \mathbb{E}_{\mathcal{P}} Q_1\| + \|\bar{Q}_2 - \mathbb{E}_{\mathcal{P}} Q_2\| \right] + \max_{s', a'} \gamma \|\mathbb{E}_{\mathcal{P}} Q_1 - \mathbb{E}_{\mathcal{P}} Q_2\|$$

Since Q function almost surely converge under exhaustive sampling we have

$$\max_{s', a'} \gamma \left\| \mathbb{E}_{\mathcal{P}} Q_1 - \mathbb{E}_{\mathcal{P}} Q_2 \right\| \leq \gamma \left\| Q_1 - Q_2 \right\|_{\infty} \quad (13)$$

From equation 12 and equation 13 we have after t time steps

$$\left\| \mathcal{T}Q_1 - \mathcal{T}Q_2 \right\|_{\infty} \leq 2c_0 + \gamma \left\| Q_1 - Q_2 \right\|_{\infty}$$

Let R_{max} and R_{min} be the maximum and minimum reward values. Then we have that

$$\left\| Q_1 - Q_2 \right\|_{\infty} \leq \frac{\gamma}{1-\gamma} R_{max} - R_{min}.$$

Thus for any $\epsilon \geq 0$ by choosing a γ such there exists a t' such that $\forall t \geq t'$

$$\|Q^t - Q^*\|_{\infty} \leq \epsilon$$

This concludes the proof of Theorem 1. \square

A.2 PROOF OF THEOREM 2

Theorem 2. Let $Q_{\mathcal{E}}^{t+1}(s_t, a_t) = r(s_t, a_t) + \gamma \sum_{s \in \mathcal{S}} \mathbb{P}(s|s_t, a_t) \max_a Q_{\mathcal{E}}^t(s, a), \forall (s_t, a_t) \in \mathcal{S} \times \mathcal{A}$ be the update rule under exhaustive sampling, and Q^t be the Q function updated according to Hamiltonian Q -Learning, i.e. by (9)-(10). Then, for any given $\tilde{\epsilon} \geq 0$, there exists $n_{\mathcal{H}}, t' > 0$, such that $\|Q^t - Q_{\mathcal{E}}^t\|_{\infty} \leq \tilde{\epsilon} \forall t \geq t'$.

Proof of Theorem 2. Note that at each time step we attempt to recover the matrix $Q_{\mathcal{E}}^t$, i.e., Q function time time t under exhaustive sampling though a matrix completion method starting from \hat{Q}^t , which is the Q updated function at time t using Hamiltonian Q -Learning. From Theorem 4 in (Chen & Chi, 2018) we have that $\forall t \geq t'$ there exists some constant $\delta > 0$ such that when the updated Q function a \hat{Q}^t satisfy

$$\left\| \hat{Q}^t - Q_{\mathcal{E}}^t \right\|_{\infty} \leq c$$

where c is some positive constant then reconstructed (completed) matrix Q^t satisfies

$$\left\| Q^t - Q_{\mathcal{E}}^t \right\|_{\infty} \leq \delta \left\| \hat{Q}^t - Q_{\mathcal{E}}^t \right\|_{\infty} \quad (14)$$

for some $\delta > 0$. This implies that when the initial matrix used for matrix completion is sufficiently close to the matrix we are trying to recover matrix completion iterations converge to a global optimum. From the result of Theorem 1 we have for any given $\epsilon \geq 0$, there exists $n_{\mathcal{H}}, t' > 0$ such that $\forall t \geq t'$

$$\left\| \hat{Q}^t - Q^* \right\|_{\infty} \leq \epsilon \quad (15)$$

Recall that under the update equation $Q_{\mathcal{E}}^{t+1}(s_t, a_t) = r(s_t, a_t) + \gamma \sum_{s \in \mathcal{S}} \max_a Q_{\mathcal{E}}^t(s, a), \forall (s_t, a_t) \in \mathcal{S} \times \mathcal{A}$ we have that $Q_{\mathcal{E}}$ almost surely converge to the optimal Q^* . Thus there exists a t^\dagger such that $\forall t \geq t^\dagger$

$$\left\| Q_{\mathcal{E}}^t - Q^* \right\|_{\infty} \leq \epsilon$$

Let $t^\ddagger = \max\{t^\dagger, t'\}$. Then from triangle inequality we have that

$$\left\| \hat{Q}^t - Q_{\mathcal{E}}^t \right\|_{\infty} \leq \left\| \hat{Q}^t - Q^* \right\|_{\infty} + \left\| Q_{\mathcal{E}}^t - Q^* \right\|_{\infty} \leq 2\epsilon.$$

Thus from equation 14 we have that

$$\left\| Q^t - Q_{\mathcal{E}}^t \right\|_{\infty} \leq 2\delta\epsilon$$

This concludes the proof of Theorem 2. \square

B ADDITIONAL EXPERIMENTAL DETAILS AND RESULTS FOR CART-POLE

Let $\theta, \dot{\theta}$ be the angle and angular velocity of the pole, respectively. Let x, \dot{x} be the position and linear velocity of the cart, respectively. Let a be the control force applied to the cart. Then, by defining m, M, l and g as the mass of the pole, mass of the cart, length of the pole and gravitational acceleration, respectively, the dynamics of cart-pole system can be expressed as

$$\begin{aligned} \ddot{\theta} &= \frac{g \sin \theta - \frac{a + ml\dot{\theta}^2 \sin \theta}{m+M} \cos \theta}{l \left(\frac{4}{3} - \frac{m \cos^2 \theta}{m+M} \right)} \\ \ddot{x} &= \frac{a + ml \left(\dot{\theta}^2 \sin \theta - \ddot{\theta} \cos \theta \right)}{m + M} \end{aligned} \quad (16)$$

State space of cart-pole system is 4-dimensional ($\mathcal{D}_s = 4$) and any state $s \in \mathcal{S}$ is given by $s = (\theta, \dot{\theta}, x, \dot{x})$. We define the range of state space as $\theta \in [-\pi/2, \pi/2]$, $\dot{\theta} \in [-3.0, 3.0]$, $x \in [-2.4, 2.4]$ and $\dot{x} \in [-3.5, 3.5]$. We consider action space to be a 1-dimensional ($\mathcal{D}_a = 1$) space such that $a \in [-10, 10]$. We discretize each dimension in state space into 5 values and action space into 10 values. This forms a Q matrix of dimensions 625×10 .

Although the differential equations (16) governing the dynamics of the pendulum on a cart system are deterministic, uncertainty of the parameters and external disturbances to the system causes the cart pole to deviate from the defined dynamics leading to a stochastic state transition. Following the conventional approach we model these parameter uncertainties and external disturbances using a multivariate Gaussian perturbation (Maithripala et al., 2016; McAllister & Rasmussen, 2017). Here we consider the co-variance of the Gaussian perturbation to be $\Sigma = \text{diag}[0.143, 0.990, 0.635, 1.346]$.

Let $s_t = (\theta_t, \dot{\theta}_t, x_t, \dot{x}_t)$ and a_t be the state and the action at time t . Then the state transition probability kernel and corresponding target distribution can be given using (7) and (8), respectively, with mean $\mu(s_t, a_t) = (\theta_t + \dot{\theta}_t \tau, \dot{\theta}_t + \ddot{\theta}_t \tau, x_t + \dot{x}_t \tau, \dot{x}_t + \ddot{x}_t \tau)$, where $\ddot{\theta}_t, \ddot{x}_t$ can be obtained from (16) by substituting $\theta_t, \dot{\theta}_t, a_t$, and co-variance $\Sigma(s_t, a_t) = \Sigma$.

Our simulation results use the following value for the system parameters - $m = 0.1kg$, $M = 1kg$, $l = 0.5m$ and $g = 9.8ms^{-2}$. We take 100 HMC samples during the update phase. We use trajectory length $L = 100$ and step size $\delta l = 0.02$. We randomly initialize the Q matrix using values between 0 and 1. We provide additional comparison heat maps for first two dimensions $\theta, \dot{\theta}$ with fixed x, \dot{x} .

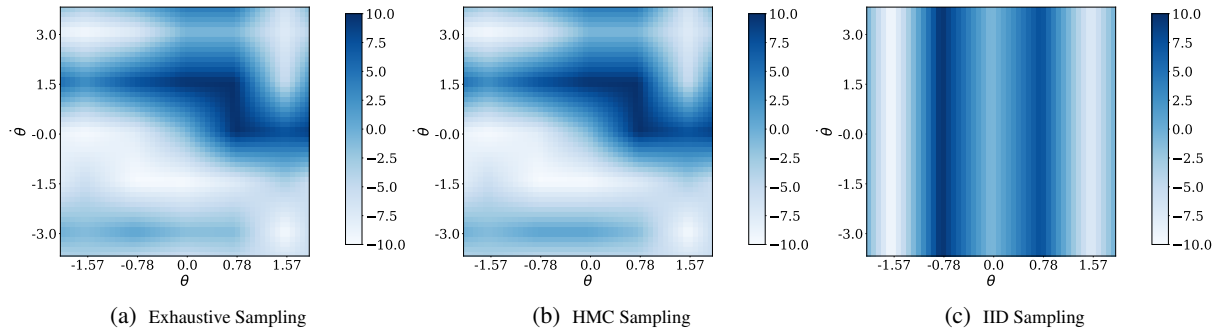


Figure 4: Figure 4(a), 4(b) and 4(c) show policy heat maps for Q -Learning with exhaustive sampling, Hamiltonian Q -Learning and Q -Learning with IID sampling, respectively.

Further, we provide additional comparison heat maps for last two dimensions x, \dot{x} with fixed $\theta, \dot{\theta}$.

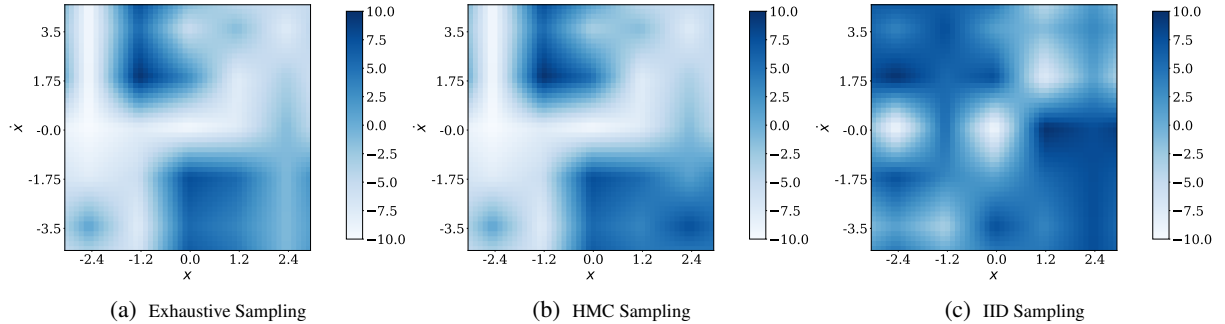


Figure 5: Figure 5(a), 5(b) and 5(c) show policy heat maps for Q -Learning with exhaustive sampling, Hamiltonian Q -Learning and Q -Learning with IID sampling, respectively.

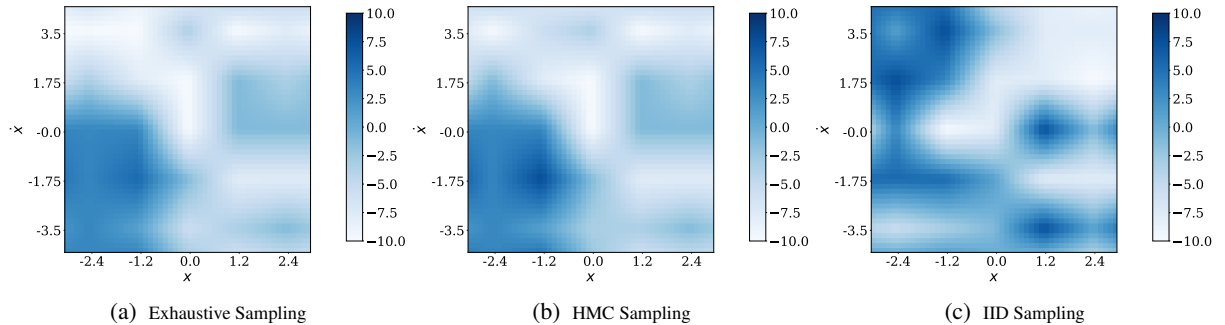


Figure 6: Figure 6(a), 6(b) and 6(c) show policy heat maps for Q -Learning with exhaustive sampling, Hamiltonian Q -Learning and Q -Learning with IID sampling, respectively.

Table 1: Notations

Notations	Description	Value
m	total mass	1.03 kg
\mathcal{I}_{in}	inner body moment of inertia	0.5 kg m ²
\mathcal{I}_{out}	outer body moment of inertia	0.174 kg m ²
r	radius	0.08 m
L	length of the flap	0.09 m
d_f	submersible depth of the flap	0.044 m
d_b	submersible depth of the body	0.02 m
β	angular location of the flap	30°
ψ	maximum open angle of the flap	20°
C_f	drag coefficient of the flap	2
C_b	drag coefficient of the body	2
ρ	water density	1027 kg m ³

C UNDER WATER GLIDER DYNAMICS

By assuming that the glider’s motion is restricted to an horizontal plane (Refael & Degani, 2019), we let x, y and θ denote its center of mass position and heading angle, respectively. Then we can define the 6-dimensional state vector for this system as $s = (x, y, \dot{x}, \dot{y}, \theta, \dot{\theta})$ and the action a as a scalar control input to the glider. Also, to accommodate dynamic perturbations due to the ocean current, other external disturbances and parameter uncertainties, we assume that the probabilistic state transition is governed by a multivariate Gaussian. We consider that the motion of the glider is restricted to a horizontal plane. Let x, y and θ be the coordinates of the center of mass of glider and heading angle respectively. By introducing $q = [x \ y \ \theta]^T$, the dynamics of the glider can be expressed as

$$M\ddot{q} = RF_f + F_b + \tau$$

where

$$\begin{aligned}
M &= \text{diag} \begin{bmatrix} m \\ m \\ \mathcal{I}_{in} + \mathcal{I}_{out} \end{bmatrix}; \quad R = \begin{bmatrix} \cos \theta & -\sin \theta & 0 \\ \sin \theta & \cos \theta & 0 \\ 0 & 0 & 1 \end{bmatrix} \\
F_f &= \begin{bmatrix} \alpha_f \dot{\theta}^2 \text{sgn}(\dot{\theta}) \sin(\beta + \psi) \\ \alpha_f \dot{\theta}^2 \cos(\beta + \psi) \\ 0 \end{bmatrix}; \quad F_b = -\alpha_b \sqrt{\dot{x}^2 + \dot{y}^2} \begin{bmatrix} \dot{x} \\ \dot{y} \\ 0 \end{bmatrix}; \quad \tau = \begin{bmatrix} 0 \\ 0 \\ -\mu_f \text{sgn}(\dot{\theta}) \dot{\theta}^2 - \mathcal{I}_{in} u \end{bmatrix} \\
\alpha_f &= \frac{1}{2} \rho C_f d_f L \left(r^2 + \left(\frac{L}{2} \right)^2 + rL \cos \psi \right); \quad \mu_f = \alpha_f \left(\frac{L}{2} + r \cos \psi \right); \quad \alpha_b = \frac{1}{2} C_b d_b \pi r \\
\alpha_b &= 0.005; \quad \alpha_f = 0.062; \quad \mu_f = 0.0074; \quad \sigma = 2.5.
\end{aligned}$$

Our simulation results use system parameter values from Table 1. We define the range of state and action space as $x, y \in [-10, 10]$, $\dot{x}, \dot{y} \in [-25, 25]$, $\theta \in [-\pi, \pi]$, $\dot{\theta} \in [-3, 3]$, and $a \in [-1, 1]$, respectively and then discretizing each state dimension into 5 distinct values and the action space into 5 distinct values, we have a Q matrix of size 15625×5 . Also, we assume that the state transition kernel is given by a multivariate Gaussian with zero mean and covariance $\Sigma = \text{diag}[11.111, 69.444, 11.111, 69.444, 0.143, 0.990]$. After initializing the Q matrix using randomly chosen values from $[0, 1]$, we sample state-action pairs independently with probability $p = 0.5$ at each iteration. Also, we assume $\sigma = 2.5$, $\lambda = 0.1$, $\mathcal{C} = \text{diag}[1, 0]$. We take 100 HMC samples during the update phase. We use trajectory length $L = 100$ and step size $\delta l = 0.02$.

We provide additional comparison heat maps for first two dimensions x, y with fixed $\dot{x}, \dot{y}, \theta, \dot{\theta}$.

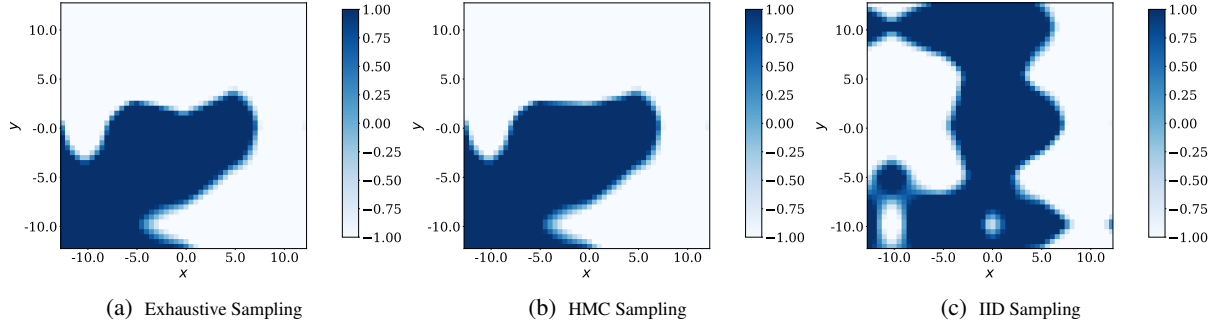


Figure 7: Figure 7(a), 7(b) and 7(c) show policy heat maps for Q -Learning with exhaustive sampling, Hamiltonian Q -Learning and Q -Learning with IID sampling, respectively.

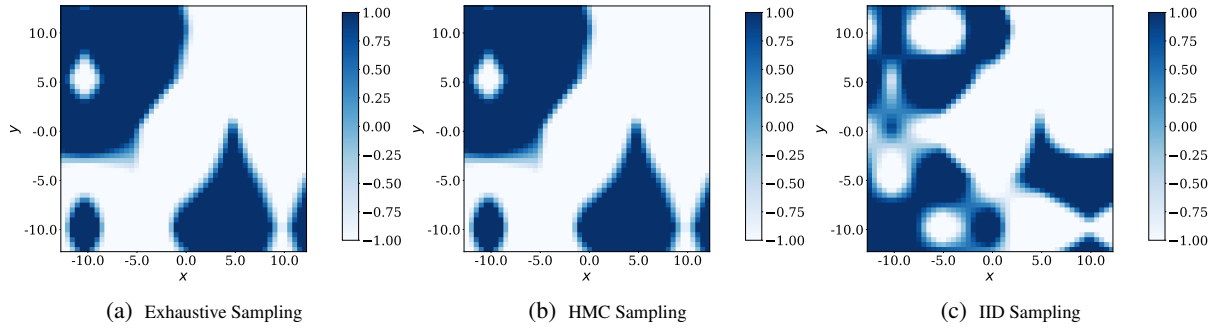


Figure 8: Figure 8(a), 8(b) and 8(c) show policy heat maps for Q -Learning with exhaustive sampling, Hamiltonian Q -Learning and Q -Learning with IID sampling, respectively.

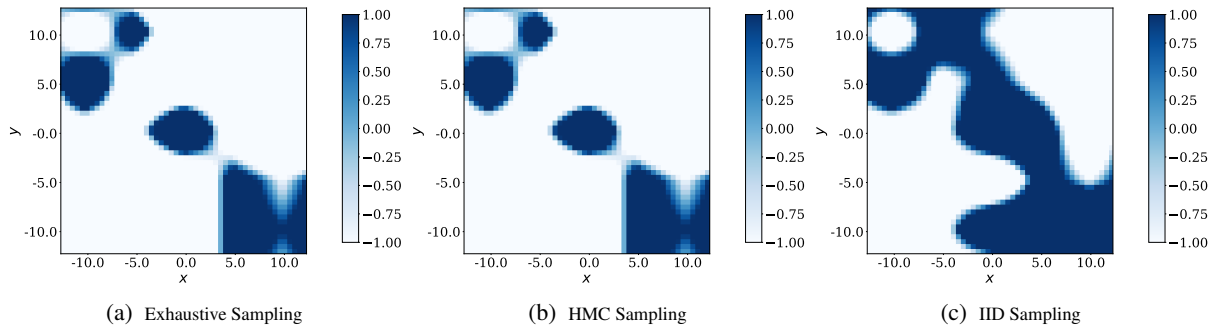


Figure 9: Figure 9(a), 9(b) and 9(c) show policy heat maps for Q -Learning with exhaustive sampling, Hamiltonian Q -Learning and Q -Learning with IID sampling, respectively.